Tunable Multi-Band Non-Reciprocal Bandpass Filters

Dakotah Simpson[1], Photos Vryonides[2,3], Symeon Nikolaou[2,3], Dimitra Psychogiou[4,5]
[1]ECEE Department, University of Colorado Boulder, USA
[2]Frederick Research Center, Cyprus
[3]Frederick University, Cyprus
[4]School of Engineering, University College Cork, Ireland
[5]Tyndall National Institute, Ireland
Dakotah.Simpson@colorado.edu, {p.vryonides, s.nikolaou}@frederick.ac.cy, DPsychogiou@ucc.ie

2022 IEEE/MTT-S International Microwave Symposium - IMS 2022 | 978-1-6654-9613-1/22/$31.00 ©2022 IEEE | DOI: 10.1109/IMS37962.2022.9865607

***Abstract*—Multi-band non-reciprocal bandpass filters (BPFs) with reconfigurable transfer function characteristics are reported. They are based on *N* in-series cascaded multi-resonant cells (MRCs) that each comprise two non-resonating junctions and *K* frequency-tunable resonators resulting in an N^{th}-order *K*-band BPF response. Non-reciprocity is introduced by modulating the resonators' resonant frequencies in both time and space. This is achieved by modulating the capacitance of constituent resonators with DC and AC signals, where the AC signals are progressively phase-shifted from one MRC to the next. The BPF can be tuned in frequency and in the direction of propagation. For practical demonstration purposes, a 3rd-order dual-band lumped-element prototype was designed and tested for center frequencies of 198 MHz and 245 MHz. It demonstrated maximum isolation levels of 26.1 and 35.9 dB and center frequency tuning ranges up to 1.1:1.**

***Keywords*—bandpass filter, isolator, multi band, non-reciprocal filter, non-reciprocity, spatiotemporal modulation, tunable filter.**

I. Introduction

Non-reciprocal components are fundamental elements of most microwave communication, radar, and instrumentation systems due to their role in protecting sensitive devices from reflected high-power signals. Moreover, they facilitate the elementary function of separating the transmit and receive channels in full-duplex radios. Their practical deployment is conventionally performed using bulky magnetically-biased ferromagnetic materials. Thus, recent research efforts have been focusing on removing magnets from non-reciprocal devices using a number of methods. These include i) developing materials with inherent magnetization (i.e., self-biased materials) [1], ii) incorporating transistors or op-amps within RF circuits [2]-[5], and iii) modulating circuits in both time and space (i.e., spatiotemporal modulation, STM) [6]-[10].

STM has recently become a popular method for the realization of RF co-designed isolators and filtering devices [7]-[10]. The method was first successfully shown in filtering circulator devices through the modulation of the resonant frequencies of resonators that were arranged in ring configurations [6]. However, these initial devices were low-order and resulted in low selectivity and high insertion loss (IL) up to 10 dB. Next, STM was used in two-port BPFs in [7]-[10] by modulating the filters' resonators with phase-progressed low frequency ($<f_{RF}$) AC signals. However, all non-reciprocal filters presented to date have been limited to a single passband without mention of how to extend to multi-band transfer functions, which is paramount in modern RF front-ends. Furthermore, only two have demonstrated tuning capabilities [7], [8].

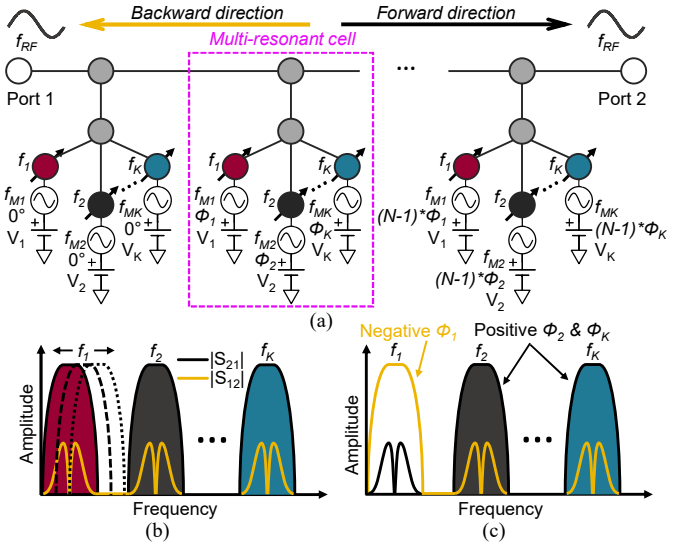

Fig. 1. Tunable multi-band non-reciprocal BPF concept. (a) Schematic of an N^{th}-order *K*-band BPF; colored circles: frequency-tunable resonators, white circles: RF input and output, gray circles: non-resonating junctions, black lines: impedance inverters. (b) Conceptual response showing center frequency tuning. (c) Conceptual response showing change of direction of propagation.

In light of these limitations, this work presents for the first time a new class of a multi-band non-reciprocal BPFs that are tunable in terms of center frequency and direction of propagation. Multi-band operation is facilitated through the use of multi-resonant cells (MRCs). STM is used to create non-reciprocity across the filter by modulating the BPF's resonators with progressively phase-shifted AC signals. The remainder of this manuscript is organized as follows. Section II details the operational and design principles of the multi-band BPF. In Section III, a dual-band prototype is illustrated. Finally, the findings of this work are outlined in Section IV.

II. Theoretical Background

The schematic and conceptual responses of the multi-band non-reciprocal BPF are depicted in Fig. 1. It is based on the cascade of *N* MRCs that each comprises *K* frequency-tunable bandpass resonators (colored circles) connected together

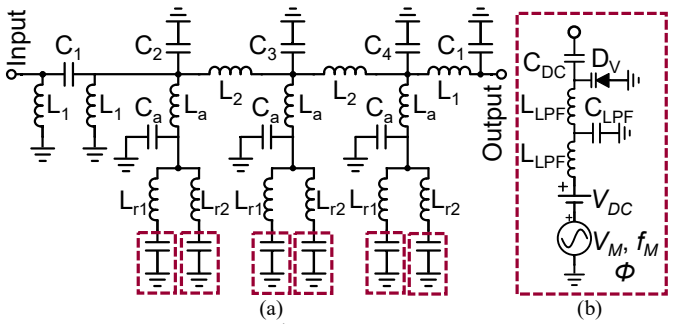

Fig. 2. Circuit-schematic of a 3rd-order (N=3) dual-band (K=2) non-reciprocal BPF. (a) Overall architecture. (b) Detailed schematic of the biasing circuitry.

through two non-resonating junctions (gray circles) and static impedance inverters (black lines). Each resonator in an MRC resonates at a different frequency (e.g., f_K) and contributes a pole to its corresponding passband. All MRCs have an equal number of resonators resulting in an N^{th}-order K-band response. The resonant frequencies of the resonators are controlled by applying DC and AC signals on their varactor-based capacitors. Whereas the DC voltage determines the average capacitance and resonant frequency of the resonator, the AC signal modulates the capacitance to impart directionality of the signal propagation throughout the BPF. As a unique advantage to be highlighted for the proposed architecture, the resonators and passbands operate independently, so the required DC and AC signals can be found separately. As shown in Fig. 1(a), there is a phase shift between the resonators for a given passband so that the circuit is not only modulated in time but also in space.

The modulating AC signal parameters, namely the voltage V_M, frequency f_M, and phase shift between resonators Φ, must be suitably chosen through parametric analysis. As shown in Fig. 1(b), a K-band transfer function in the forward direction of propagation and a cancellation of the RF signals in the reverse direction can be obtained. Fig. 1(b) also shows that the center frequency of a passband can be tuned independently of the others. This is realized by synchronously tuning the DC voltage applied on the resonators of each band. Furthermore, the proposed filter concept also allows for reconfigurability of the direction of propagation (see Fig. 1(c)) which is controlled by the sign of the progressive phase shift imparted on its resonators. A positive phase shift results in a forward direction of propagation, whereas a negative phase shift results in a backward direction of propagation. This trait can also be used to reconfigure the number of passbands present in each direction of propagation.

To demonstrate the operational principles of the concept, an example circuit and its simulated responses are detailed next. Fig. 2 shows a lumped-element (LE) circuit implementation of the block diagram in Fig. 1(a) for N = 3 and K = 2 (i.e., a 3rd-order dual-band BPF). The static impedance inverters have been implemented with first-order pi-type LE networks and elements have been combined where possible to reduce the number of components. Furthermore, the resonators have been incorporated with their preceding impedance inverters through parallel-to-series conversions and are equivalently realized as series-type LC resonators to reduce the number of components. The resonators' capacitors are replaced with the network in Fig.

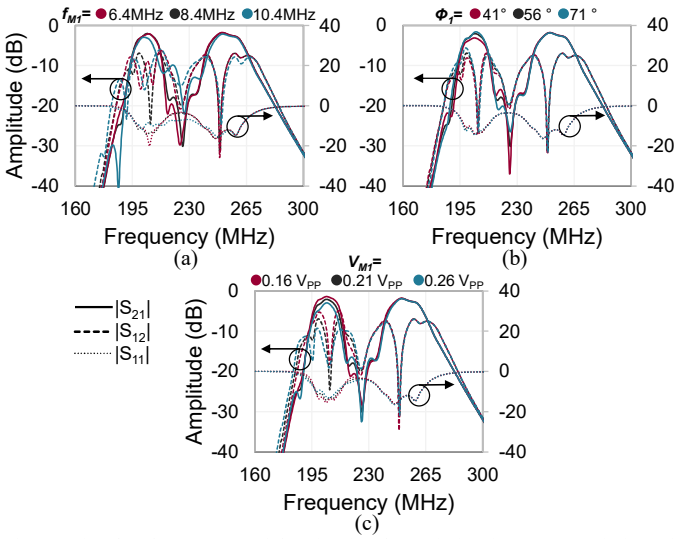

Fig. 3. Simulated responses of the circuit schematic in Fig. 2. (a) Variation of modulation frequency. (b) Variation of phase offset. (c) Variation of the amplitude of the modulation signal. The component values used are: L_1=42nH, L_2=47.7nH, L_a=24.2nH, L_{r1}=100nH, L_{r2}=58nH, L_{LPF}=350nH, C_1=12.7pF, C_2=31.2pF, C_3=41.4pF, C_4=43.9pF, C_a=21pF, C_{DC}=82pF, and C_{LPF}=82pF.

2(b) that consists of a varactor diode (D_V) that is AC- and DC-biased through a lowpass filter (L_{LPF} and C_{LPF}) with a cut-off frequency much lower than the passband's center frequency. A DC-blocking capacitor (C_{DC}) is also added at the input of the network to block the DC current from entering other parts of the filter and connecting circuitry.

The design of the BPF is performed as follows. First, the values of the components are determined by designing a static reciprocal multi-band BPF with the desired center frequencies and bandwidths (BWs), as for example in [11]. Afterwards, the resonators' capacitors are replaced with DC-biased varactor diodes and the bias circuitry in Fig. 2(b). The varactors should be chosen and biased such that the resonator capacitance is within the midrange of the achievable capacitances so that the frequency can be tuned in both directions. Next, the AC modulation signal parameters are found through parametric analysis to attain low in-band IL in the forward direction and high isolation in the reverse direction. Since the bands operate independently, their parameters can be found separately.

To illustrate the aforementioned design steps, a 3rd-order dual-band BPF is designed with bands centered at 200 and 250 MHz with BWs of 15 and 20 MHz, respectively. Ideal LEs and Skyworks SMV1413 varactor diodes are used for the circuit in Fig. 2. The responses of the filter under different AC

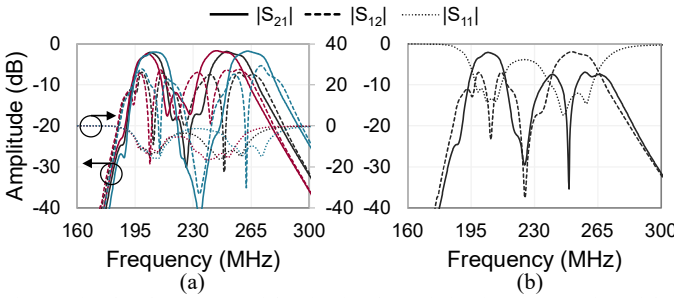

Fig. 4. Simulated responses of the circuit schematic in Fig. 2. (a) Tuning of the upper passband. (b) Reconfiguration of directionality.

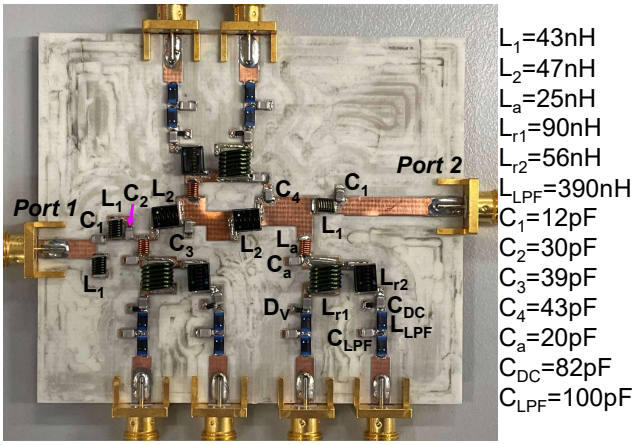

(a)

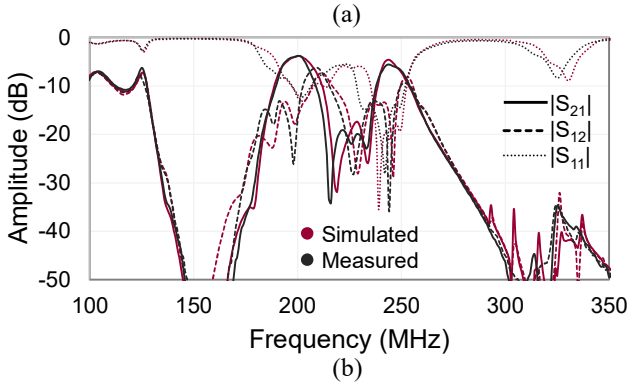

(b)

Fig. 5. (a) Manufactured prototype and list of component values. (b) Comparison of RF measured and EM simulated responses of the prototype.

modulation parameters for the first passband are shown in Fig. 3. For briefness, the analysis is only shown for the first passband and the parameters of the second passband have been found using the same method. Fig. 3(a) illustrates the BPF response as f_{MI} changes and all other parameters are kept constant. As can be seen, too low or high of an f_M leads to low isolation (~15 dB) in the reverse direction and a high f_M also results in deformation of the passband. A modulation frequency of about 8.4 MHz is found to be optimal. In Fig. 3(b), the phase progression, Φ_1, is changed. When Φ_1 is too low an increase in IL is noticed. On the other hand, when Φ_1 is too high the in-band isolation is slightly affected. Lastly, Fig. 3(d) shows the BPF response when the modulation voltage, V_{MI}, is varied. A low V_{MI} results in lower IL but also lower isolation, whereas a high V_{MI} results in high IL and low isolation. As shown while altering these parameters, the second passband remains unchanged.

The multi-band non-reciprocal BPF can be tuned in terms of band frequency and direction of propagation. Fig. 4 shows both of these levels of tuning. In Fig. 4(a), the center frequency of the upper passband is tuned by synchronously tuning the DC voltage on its constituent varactor diodes. As it can be seen, a high level of isolation is obtained while the band is tuned. Fig. 4(b) plots the reconfiguration of the direction of propagation of the upper passband by changing the sign of the phase progression of the AC signals biasing its resonators. This has resulted in one band being propagated in the forward direction and can be used to control the number of active bands.

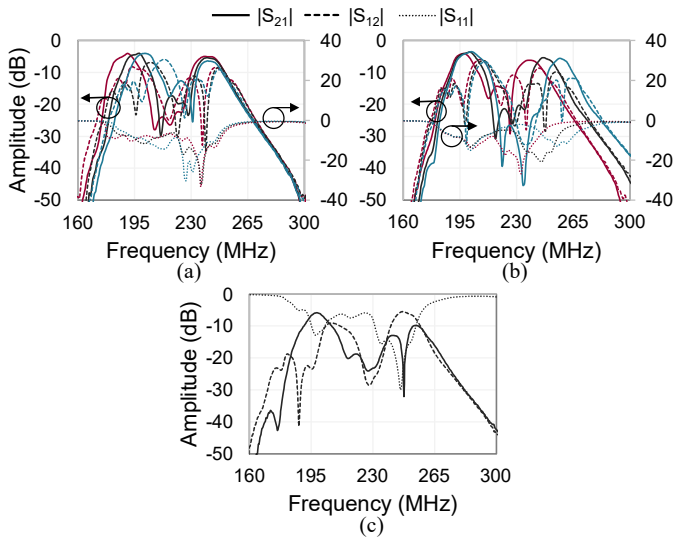

Fig. 6. Measured tuning responses of the prototype. (a) Frequency tuning of the lower passband. (b) Frequency tuning of the upper passband. (c) Reconfiguration of the direction of propagation.

III. Experimental Validation

To validate the tunable multi-band non-reciprocal BPF concept, a 3rd-order dual-band prototype was developed and measured. It was designed to have passbands centered at 200 and 250 MHz with BWs of 15 MHz and 18 MHz, respectively. A photograph and a list of its components are shown in Fig. 5 (a). SMV1413 varactors from Skyworks were utilized as tuning elements. They were AC- and DC-biased through clock-synced waveform generators that were connected to the PCB via SMA connectors. The RF responses of the prototype were measured using a Keysight N5224A PNA.

One RF-measured response is plotted with its corresponding EM-simulated response in Fig. 5(b). The measured center frequencies of the two passbands are 198 MHz and 245 MHz. The BWs are measured to be 14.5 MHz and 14 MHz. The prototype exhibits minimum in-band ILs of 3.7 and 5.5 dB, respectively, in the forward direction. Moreover, it exhibits measured maximum isolations of 26.1 and 35.9 dB in the reverse direction. Fig. 6 demonstrates the tuning capabilities of the prototype. Fig. 6(a) depicts the frequency tuning of the lower passband. It can be tuned in the range 188-202 MHz (1.1:1 tuning ratio). Fig. 6(b) illustrates the frequency tuning of the upper passband from 237 MHz to 257 MHz (1.1:1 ratio). Switching the direction of propagation is shown in Fig. 6(c). This has also changed the number of active bands in the forward direction from two to one and can be used to control the number of active passbands in the forward direction.

IV. Conclusion

A new type of non-reciprocal multi-band BPF has been reported. It is based on the cascade of multi-resonant cells, where the number of resonators in each cell determines the number of passbands. Directionality is imparted on the circuit by applying low-frequency ($< f_{RF}$) phase-shifted AC signals on the resonators of each band. By simultaneously varying the DC voltages on a band's resonators, the passband can be tuned in

frequency. By changing the sign of the phase progression of the modulation signals, the direction of propagation can be reconfigured. For validation, a 3rd-order dual-band prototype was developed and measured. It demonstrated maximum isolation levels of 26.1 and 35.9 dB in its two bands, respectively, and frequency tuning ratios of 1.1:1 for both bands.

ACKNOWLEDGMENT

This work has been supported in part by NSF project No. ECCS-1941315 and by SFI project No. 20/RP/8334.

REFERENCES

[1] G. Hamoir, L. Piraux, and I. Huynen, "Control of microwave circulation using unbiased ferromagnetic nanowires arrays," *IEEE Trans. Magnetics*, vol. 49, no. 7, pp. 4261-4264, July 2013.

[2] S. W. Y. Mung and W. S. Chan, "Active three-way circulator using transistor feedback network," *IEEE Microw. Wireless Compon. Lett.*, vol. 27, no. 5, pp. 476-478, May 2017.

[3] A. Ashley and D. Psychogiou, "RF co-designed bandpass filters/isolators using nonreciprocal resonant stages and microwave resonators," *IEEE Trans. Microw. Theory Techn.*, vol. 69, no. 4, pp. 2178-2190, Apr. 2021.

[4] A. Ashley and D. Psychogiou, "X-band quasi-elliptic non-reciprocal bandpass filters (NBPFs)," *IEEE Trans. Microw. Theory Techn.*, vol. 69, no. 7, pp. 3255-3263, Jul. 2021.

[5] A. Ashley and D. Psychogiou, "Non-reciprocal MMIC-based dual-band bandpass filters," *2021 IEEE MTT-S Intern. Microw. Symp. (IMS)*, 2021, pp. 100-103.

[6] N. A. Estep, D. L. Sounas, and A. Alù, "Magnetless microwave circulators based on spatiotemporally modulated rings of coupled resonators," *IEEE Trans. Microw. Theory Techn.*, vol. 64, no. 2, pp. 502 518, Feb. 2016.

[7] D. Simpson and D. Psychogiou, "Magnet-less non-reciprocal bandpass filters with tunable center frequency", *Proc. 49th European Microwave Conference (EuMC)*, 2019, Paris, France.

[8] D. Simpson and D. Psychogiou, "Fully-reconfigurable non-reciprocal bandpass filters," *2020 IEEE MTT-S Intern. Microw. Symp. (IMS)*, Los Angeles, CA, USA, 2020, pp. 807-810.

[9] X. Wu, M. Nafe, A. A. Melcón, J. Sebastián Gómez-Díaz and X. Liu, "A non-reciprocal microstrip bandpass filter based on spatio-temporal modulation," *2019 IEEE MTT-S Intern. Microw. Symp. (IMS)*, Boston, MA, USA, 2019, pp. 9-12.

[10] X. Wu, M. Nafe, A. Á. Melcón, J. S. Gómez-Díaz, and X. Liu, "Frequency tunable non-reciprocal bandpass filter using time-modulated microstrip λg/2 resonators," *IEEE Trans. Circ. Syst. II*, vol. 68, no. 2, pp. 667-671, Feb. 2021.

[11] R. Gómez-García, A. C. Guyette, D. Psychogiou, E. J. Naglich, and D. Peroulis, "Quasi-elliptic multi-band filters with center-frequency and bandwidth tunability," *IEEE Microw. Wireless Compon. Lett.*, vol. 26, no. 3, pp. 192-194, Mar. 2016.